IEEE Access
Multidisciplinary | Rapid Review | Open Access Journal

SPECIAL SECTION ON ADVANCED DATA ANALYTICS FOR LARGE-SCALE COMPLEX DATA ENVIRONMENTS

Received September 26, 2017, accepted November 19, 2017, date of publication December 1, 2017,
date of current version February 14, 2018.

Digital Object Identifier 10.1109/ACCESS.2017.2778947

Hyperspectral Image Denoising With Group Sparse and Low-Rank Tensor Decomposition

ZHIHONG HUANG[1], (Student Member, IEEE), SHUTAO LI[1], (Senior Member, IEEE), LEYUAN FANG[1], (Senior Member, IEEE), HUALI LI[1], (Member, IEEE), AND JÓN ATLI BENEDIKTSSON[2], (Fellow, IEEE)

[1]College of Electrical and Information Engineering, Hunan University, Changsha 410082, China
[2]Faculty of Electrical and Computer Engineering, University of Iceland, 101 Reykjavik, Iceland

Corresponding author: Huali Li (rss0310005@gmail.com)

This paper was supported in part by the National Natural Science Foundation of China under Grant 61301255, Grant 61771192, and Grant 61471167, in part by the National Natural Science Fund of China for Distinguished Young Scholars under Grant 61325007, in part by the National Natural Science Fund of China for International Cooperation and Exchanges under Grant 61520106001, and in part by the Science and Technology Plan Project Fund of Hunan Province under Grant 2015WK3001 and Grant 2017RS3024.

ABSTRACT Hyperspectral image (HSI) is usually corrupted by various types of noise, including Gaussian noise, impulse noise, stripes, deadlines, and so on. Recently, sparse and low-rank matrix decomposition (SLRMD) has demonstrated to be an effective tool in HSI denoising. However, the matrix-based SLRMD technique cannot fully take the advantage of spatial and spectral information in a 3-D HSI data. In this paper, a novel group sparse and low-rank tensor decomposition (GSLRTD) method is proposed to remove different kinds of noise in HSI, while still well preserving spectral and spatial characteristics. Since a clean 3-D HSI data can be regarded as a 3-D tensor, the proposed GSLRTD method formulates a HSI recovery problem into a sparse and low-rank tensor decomposition framework. Specifically, the HSI is first divided into a set of overlapping 3-D tensor cubes, which are then clustered into groups by K-means algorithm. Then, each group contains similar tensor cubes, which can be constructed as a new tensor by unfolding these similar tensors into a set of matrices and stacking them. Finally, the SLRTD model is introduced to generate noise-free estimation for each group tensor. By aggregating all reconstructed group tensors, we can reconstruct a denoised HSI. Experiments on both simulated and real HSI data sets demonstrate the effectiveness of the proposed method.

INDEX TERMS Hyperspectral image, denoising, sparse and low-rank tensor decomposition, nonlocal similarity.

I. INTRODUCTION

Hyperspectral image has attracted much attention in many application fields, including the land use analysis, urban planning, and mapping [1]. In image acquisition and transmission process, HSI is inevitably corrupted by various types of noise, which will seriously deteriorate the performances in subsequent process, including unmixing [2], [3], target detection [4], [5], classification [6], [7], and super-resolution [8]. Therefore, it is essential to develop effective HSI reconstruction techniques. During the past decades, many denoising methods have been developed under different frameworks [9]. On the one hand, by regarding each band as one independent 2D image, the traditional 2D denoising methods are utilized in a bandwise manner (e.g., wavelet-based method [10], [11], KSVD [12], [13] and block-matching 3-D filtering (BM3D) [14]). However, the bandwise methods ignore the correlations among different spectral bands, which leads to a relatively low-quality recovery result. On the other hand, researchers have paid much attention to treat the HSI as a 3D data cube. By using multilinear algebra tools to treat HSI as a 3D cube, a multidimensional Wiener filtering (MWF) [15] is proposed to recover the image. Liu *et al.* [16] utilize a powerful multilinear algebra model (PARAFAC) to reconstruct the HSI. The above methods can achieve a good denoising performance. However, they only assume that HSI is degraded by Gaussian noise.

In real applications, the acquired HSI is usually corrupted by mixed noise, such as Gaussian noise, impulse noise, stripes, dead lines and so on, seriously degrading the quality

of image. To remove the above mentioned mixed noise, some denoising methods have been developed [17]–[22]. Liu *et al.* [17] propose a weighted joint sparse representation (WJSR) model to remove the mixed noise, which utilizes the joint sparse representation framework to combine the global prior with the sparse errors. Incorporated with a detector, the nonlocal mean filter [18] is developed to suppress the mixed noise. Recently, sparse and low-rank matrix decomposition (SLRMD), which is idealized as low-rank matrix recovery (LRMR) model, has been popularly used in removing the mixed noise [19]. Fan *et al.* [20] propose a modified version of LRMR (SS-LRR) method, by superpixel segmentation. Wang *et al.* [21] propose a group low-rank representation (GLRR) method, which first clusters similar patches into a group and the similar patches are jointly reconstructed using LRR. He *et al.* [22] propose a total-variation regularized low-rank matrix factorization (LRTV) model, by utilizing total variation regularization. In general, the above methods provide promising results. However, these methods process the 3D HSI data as a 2D matrix, which fails to fully explore spatial and spectral information in a 3D HSI data.

Tensor can jointly process the 3D data, and recently, some tensor based methods have been developed for HSI denoising [23]–[25]. Guo *et al.* [23] develop a rank-1 tensor decomposition (R1TD) model to remove the mixed noise. A denoised HSI is then obtained by combining the rank-1 tensors using an eigenvalue intensity sorting and reconstruction technique. Fan *et al.* [24] propose a low-rank tensor recovery (LRTR) method, which adopts the new tensor based singular value decomposition and tensor nuclear norm to suppress the mixed noise. Wu *et al.* [25] develop a structural tensor total variation-regularized weighted nuclear norm minimization (STWNNM) model for HSI denoising, which exploits the spectral information by shrinking different eigenvalues with different weights.

In this paper, we propose a group tensor based method termed as the group sparse and low-rank tensor decomposition (GSLRTD) method for the mixed noise denoising. In GSLRTD, a corrupted HSI is first divided into 3D cubes, and nonlocal similar 3D cubes are clustered to create the corresponding 3D tensor. Each group tensor has homogeneous structures and thus follows the low rank property, which can be used to well reconstruct the corrupted structures. Then, a sparse and low-rank tensor decomposition (SLRTD) algorithm is applied on each group tensor to simultaneously exploit the local and nonlocal similarity of HSI for denoising. Based on the low-rank prior knowledge of the clean HSI and the sparsity property of the sparse noise, we build our HSI restoration model based on SLRTD.

The rest of the paper is organized as follows. Low-rank matrix recovery model is presented in Section II. The proposed GSLRTD is introduced in Section III. Experimental results and analysis are reported in Section IV, and conclusions are given in Section V.

II. LOW-RANK MATRIX RECOVERY MODEL

Low-rank matrix recovery model (LRMR) [26] is proposed to recover corrupted image. It is assumed that a corrupted data matrix $D \in R^{a\times b}$ can be decomposed into the sum of a low-rank clean patch $L \in R^{a\times b}$ and a noise term $S \in R^{a\times b}$.

The noises fall into two broad categories, according to the density of their distributions: sparse noise and dense noise, in which the sparse noise mainly contains impulse noise, stripes and dead lines, and the dense noise is Gaussian noise. Fan *et al.* [20], develop the SS-LRR method to remove different types of noise and the corresponding degradation model can be defined as follows:

$$D = L + E + G \tag{1}$$

where $D \in R^{B\times P}$ and B is the number of pixels in each superpixel homogeneous region, which is reshaped into a matrix. P is the number of spectral bands. L is the clean low-rank term of homogeneous region. E represents the sparse noise term and G is the Gaussian noise term. The L, E and G all have the same size as D. In [20], the matrix nuclear norm is used as a convex relaxation of the low-rank matrix and l_1 norm is employed to characterize the sparse property. Then, the minimization problem is formulated as followed:

$$\min_{L,E} \|L\|_* + \lambda \|E\|_1, \quad s.t. \ \|D - L - E\|_F < \sigma \tag{2}$$

where λ is the balance parameter between the low-rank item and the sparse item, and σ is a constant related to the standard deviation of the Gaussian noise G. This optimization problem (2) can be solved by employing the alternating direction method (ADM) [27].

For the SS-LRR, it can only handle 2D matrix data. Since a real HSI is a three-dimensional data, the matrix based technique fails to fully utilize the spatial and spectral information.

III. PROPOSED GSLRTD MODEL FOR HSI DENOISING

To overcome the shortcoming of the matrix based technique, the tensor analysis strategy is adopted to recover corrupted HSI data, which can well exploit the three-dimensional spatial and spectral information of the HSI. Furthermore, we incorporate the nonlocal similar property into the SLRTD model to exploit spatial structural information, which can efficiently detect the mixed noise and recover the corrupted HSI. The whole procedure framework of GSLRTD method is illustrated in Fig. 1.

A. TENSOR RELATED NOTIONS

In this section, we firstly introduce some tensor related notions and preliminaries as follows. A tensor (high-order data) is denoted as Euler script letter, e.g., $\mathcal{A}$. A matrix (second-order data) is denoted as new roman letter, e.g., A, and we denote a vector (first-order data) as lowercase letters, e.g., a.

For a 3-order tensor $\mathcal{A} \in R^{n_1\times n_2\times n_3}$, its (i, j, k)-th entry is denoted as a_{ijk}. The inner product of $\mathcal{A} \in R^{n_1\times n_2\times n_3}$ and $\mathcal{B} \in R^{n_1\times n_2\times n_3}$ is denoted as. In addition, some norms of tensor

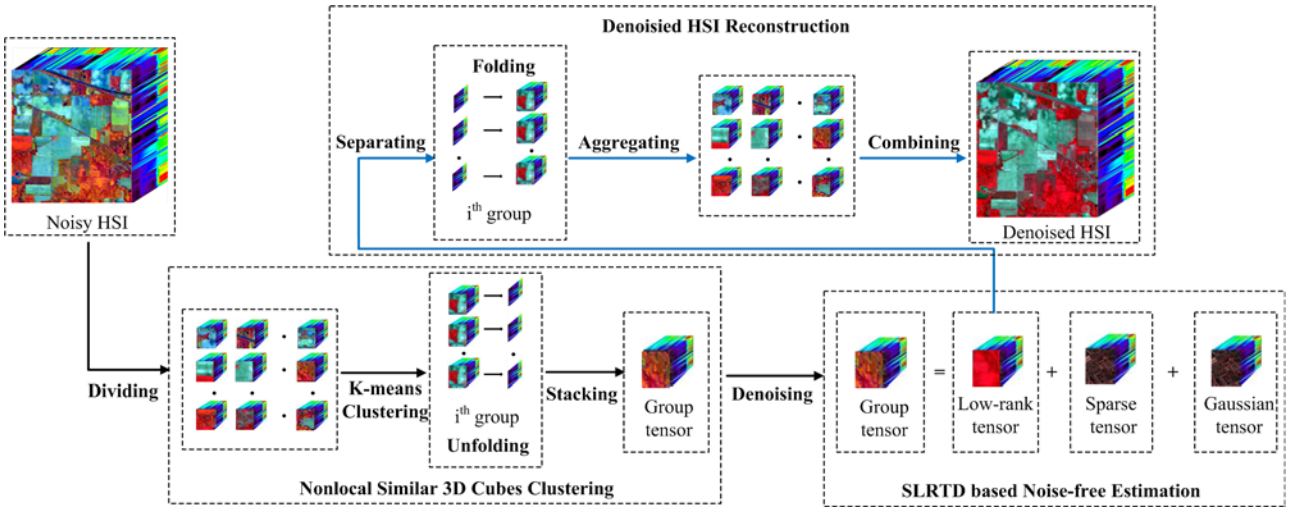

FIGURE 1. Framework of the proposed GSLRTD method.

are denoted as follows. The l_1 norm is $\|A\|_1 = \sum_{ijk} |a_{ijk}|$, the Frobenius norm is $\|A\|_F = \sqrt{\sum_{ijk} |a_{ijk}|^2}$ [28].

*Definition 1 (t-Product) [29]:*The t-product is based on block circulant matrix [29], which is a new matricization of a tensor. For $\mathcal{A} \in R^{n_1 \times n_2 \times n_3}$, its block circulant matrix has the size $n_1 n_3 \times n_2 n_3$ and it is defined as:

$$bcirc(\mathcal{A}) = \begin{pmatrix} A^{(1)} & A^{(n_3)} & \cdots & A^{(2)} \\ A^{(2)} & A^{(1)} & \cdots & A^{(3)} \\ \vdots & \vdots & & \vdots \\ A^{(n_3)} & A^{(n_3-1)} & \cdots & A^{(1)} \end{pmatrix} \tag{3}$$

There are two operators, (i.e., unfold and fold) which are separately defined as:

$$unfold(\mathcal{A}) = \begin{pmatrix} A^{(1)} \\ A^{(2)} \\ \vdots \\ A^{(n_3)} \end{pmatrix} \tag{4}$$

$$fold(unfold(\mathcal{A})) = \mathcal{A} \tag{5}$$

Given two third-order tensors $\mathcal{A} \in R^{n_1 \times n_2 \times n_3}$ and $\mathcal{B} \in R^{n_2 \times n_4 \times n_3}$, the t-product of $\mathcal{A}$ and $\mathcal{B}$ is defined to be a tensor of size $n_1 \times n_4 \times n_3$, and $*$ denotes the t-product.

$$\mathcal{A} * \mathcal{B} = fold(bcirc(\mathcal{A}) \cdot unfold(\mathcal{B})) \tag{6}$$

Definition 2: (T-SVD [30]): For $\mathcal{A} \in R^{n_1 \times n_2 \times n_3}$, it can be decomposed as:

$$\mathcal{A} = \mathcal{U} * \mathcal{S} * \mathcal{V}^T \tag{7}$$

where $\mathcal{U}$ and $\mathcal{V}$ are orthogonal tensors of size $n_1 \times n_1 \times n_3$ and $n_2 \times n_2 \times n_3$, respectively. $\mathcal{S}$ is a rectangular f-diagonal tensor of size $n_1 \times n_2 \times n_3$. This decomposition is based on computing matrix SVD in the Fourier domain.

Definition 3: (Tensor Nuclear Norm [29]): The tensor nuclear norm of $\mathcal{A} \in R^{n_1 \times n_2 \times n_3}$ is denoted as $\|\mathcal{A}\|_*$, which is the average of the nuclear norm of all the frontal slices of $\overline{\mathcal{A}}$, i.e.,$\|\mathcal{A}\|_* = \frac{1}{n_3} \sum_{i=1}^{n_3} \left\|\overline{A}^{(i)}\right\|_*$. The above mentioned tensor nuclear norm is defined in the Fourier domain. It is closely related to the nuclear norm of the block circulant matrix in the original domain. That iss $\|\mathcal{A}\|_* = \frac{1}{n_3} \sum_{i=1}^{n_3} \left\|\overline{A}^{(i)}\right\|_* = \frac{1}{n_3} \left\|\overline{A}\right\|_* = \frac{1}{n_3} \|bcirc(\mathcal{A})\|_*$.

B. NONLOCAL SIMILAR 3D CUBES CLUSTERING

In HSI, nonlocal similar 3D cubes contain abundant spatial structure information, which is beneficial to reconstruct the corrupted image. Based on this consideration, the strategy of nonlocal similarity 3D cubes clustering is adopted.

Specifically, a HSI data can be regarded as a 3D tensor $\mathcal{D} \in R^{M \times N \times P}$ with two spatial modes M, N and one spectral mode P. Firstly, the HSI is divided into overlapping 3D cubes $\{P_{i,j}\}_{1 \le i \le M-m, 1 \le j \le N-n} \subset R^{m \times n \times P}$ and sliding window step s (set as $s = 1$ in this paper), thus the number of cubes is equal to $(M - m + 1) \times (N - n + 1)$. Then, an efficient K-means algorithm [31] is utilized to cluster these similarity cubes into groups $\{Z^{(i,s)}\}_{j=1}^{J}$, $i = 1, 2, \ldots, I$, where I is the group number and J is the number of 3D cubes in the i^{th} group. The cubes in each group are unfolded to form corresponding matrices and these blocks are stacked into new group tensors $\mathcal{D}^i \in R^{mn \times P \times J}$. Therefore, the corresponding degradation model for each group tensor can be written as follows:

$$\mathcal{D}^i = \mathcal{L}^i + \mathcal{E}^i + \mathcal{G}^i \tag{8}$$

where $\mathcal{L}^i$ is the low-rank term in each group tensor. $\mathcal{E}^i$ and $\mathcal{G}^i$ separately stand for the sparse noise term, and the Gaussian noise term in each group tensor.

C. LOW-RANK PROPERTY OF GROUP TENSORS

Given a HSI $\mathcal{D} \in R^{M \times N \times P}$, the size of $\mathcal{D}$ is $M \times N \times P$, where M is the width of the image, N represents the height of the image, and P is the number of bands. The size of each 3D

cube $P_{x,y}$ is $m \times n \times P$. We can reformulate it as a 2D matrix $B_{x,y} \in R^{mn \times P}$ as follows:

$$B_{x,y} = (P_{x,y,1}, P_{x,y,2}, \ldots, P_{x,y,P}) \tag{9}$$

The low-rank property of a HSI can be achieved by a linear spectral mixing model [3]. Since HSI has high correlations among the spectral signatures (rows of $B_{x,y}$), a pixel in HSI can be represented by the linear combination of a small number of spectral endmembers, which have relatively stable spectral characteristics termed signatures. According to [3], $B_{x,y}$ can be decomposed as:

$$B_{x,y} = M \times H^T \tag{10}$$

where $H \in R^{B \times r}$ is the matrix whose columns contain pure spectral endmembers and $M \in R^{mn \times r}$ is the abundance matrix, and r is the upper bound of the number of pure spectral endmembers for $B_{x,y}$. Because the upper bound value of the number of endmember r is usually small, the rank of $B_{x,y}$ is limited, i.e., $rank(B_{x,y}) \leq r$, which means that matrix $B_{x,y}$ is of low-rank. That is the dimension of the spectral dimension in $B_{x,y}$ is lower than the number of endmembers. As shown in Fig. 2, since the similar cubes in each group are overlapping which have high spatial similarity, each group tensor has the homogeneous structure. Therefore, the clean tensor term in each group tensor region contains high correlation, which makes the clean tensor term in each group tensor region have the underlying low rank property.

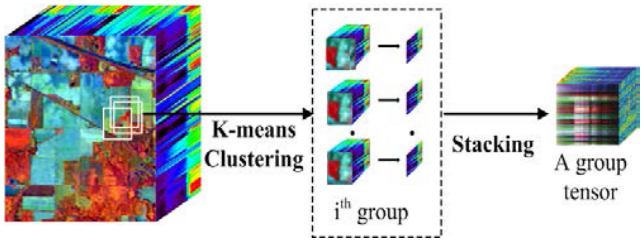

FIGURE 2. The presentation of homogeneous structure in a group tensor.

D. SLRTD DENOISING FRAMEWORK

Because tensor nuclear norm is equal to the sum of the nuclear norms of all frontal slices of $\overline{\mathcal{A}}$, we minimize $\|\mathcal{A}\|_*$, which means recovering the low-rank subspace of each frontal slice $\left\|\overline{A}\right\|_*$. With this property, tensor nuclear norm is used to depict the low-rank structure of a tensor. In addition, the number of nonzero elements of $\mathcal{E}^i$ is small, which makes $\mathcal{E}^i$ have the underlying sparse property. The l_1 norm has been demonstrated to be robust when it is used to constrain sparse noise [20]. Therefore, the tensor nuclear norm can be used as a convex relaxation of the tensor rank and l_1 norm is adopted to characterize the sparse property. The minimization problem can be reformulated as follows:

$$\min_{\mathcal{L}^i, \mathcal{E}^i} \left\|\mathcal{L}^i\right\|_* + \lambda \left\|\mathcal{E}^i\right\|_1, \quad s.t. \ \left\|\mathcal{D}^i - \mathcal{L}^i - \mathcal{E}^i\right\|_F < \sigma \tag{11}$$

where $\left\|\mathcal{L}^i\right\|_*$ is the nuclear norm of tensor $\mathcal{L}^i$ and $\|\|_F$ is the Frobenius norm. Instead of solving (11) directly, we solve the penalized form as follows:

$$\min_{\mathcal{L}^i, \mathcal{E}^i} \left\|\mathcal{L}^i\right\|_* + \lambda \left\|\mathcal{E}^i\right\|_1 + \frac{1}{2\mu} \left\|\mathcal{D}^i - \mathcal{L}^i - \mathcal{E}^i\right\|_F \tag{12}$$

where λ is the regularization parameter, which balances the relative contribution between the nuclear norm and the l_1 norm that restricts the sparsity of the sparse noise and σ represents a constant related to the standard deviation of the Gaussian noise. The performance of (12) is highly related with the two parameters λ and μ. As in [20], we set $\mu = (\sqrt{M} + \sqrt{N} + \sqrt{P})\sigma$ and $\lambda = 1/\sqrt{\max(M, N)P}$. To solve the optimization problem in (12), the alternating direction method (ADM) [27] is adopted. Therefore, problem (12) can be solved in an alternating fashion until convergence. The two subproblems to be solved in each iteration are the following:

$$\begin{aligned} \mathcal{L}^i_{k+1} &= \arg\min_{\mathcal{L}^i} \left\|\mathcal{L}^i\right\|_* + \frac{1}{2\mu} \left\|D^i - \mathcal{L}^i - \mathcal{E}^i_k\right\|_F \\ &= T_\mu(\mathcal{D}^i - \mathcal{E}^i_k) \end{aligned} \tag{13}$$

$$\begin{aligned} \mathcal{E}^i_{k+1} &= \arg\min_{\mathcal{E}^i} \lambda \left\|\mathcal{E}^i\right\|_1 + \frac{1}{2\mu} \left\|\mathcal{D}^i - \mathcal{L}^i_{k+1} - \mathcal{E}^i\right\|_F \\ &= S_{\lambda\mu}(\mathcal{D}^i - \mathcal{L}^i_{k+1}) \end{aligned} \tag{14}$$

where T_τ is the singular value shrinkage operation in the Fourier domain [29], which is defined as follows:

$$T_\tau(\mathcal{X}) = \mathcal{U} * S_\tau(\Lambda) * \mathcal{V}^T \tag{15}$$

where $\mathcal{X} = \mathcal{U} * \Lambda * \mathcal{V}^T$ is the tensor singular value decomposition [30] and $S_\tau[x] = \max(x - \tau, 0) + \max(x - \tau, 0)$ is the shrinkage operator [29]. To sum up, the procedure in detail for solving (12) is listed in Algorithm 1.

Algorithm 1 Solving Eq. (12) With ADM

Input: $\mathcal{D}^i$;
Output: $\mathcal{L}^i$, $\mathcal{E}^i$;
1: Initialize $\mathcal{L}^i$, $\mathcal{E}^i$, λ, μ;
2: **while** convergence criterion is not satisfied **do**
3: Update $\mathcal{L}^i_{k+1}$ by

$$\mathcal{L}^i_{k+1} = T_\mu(\mathcal{D}^i - \mathcal{E}^i_k)$$

4: Update $\mathcal{E}^i_{k+1}$ by

$$\mathcal{E}^i_{k+1} = S_{\lambda\mu}(\mathcal{D}^i - \mathcal{L}^i_{k+1})$$

5: **end while**
6: **return** $\hat{\mathcal{L}}^i = \mathcal{L}^i_{k+1}$, $\hat{\mathcal{D}}^i = \mathcal{D}^i_{k+1}$

E. COMPUTATIONAL COMPLEXITY ANALYSIS

The computational complexity of our GSLRTD method is as followed. The main running time is consumed by the clustering and the performing the calculation of FFT and n_3

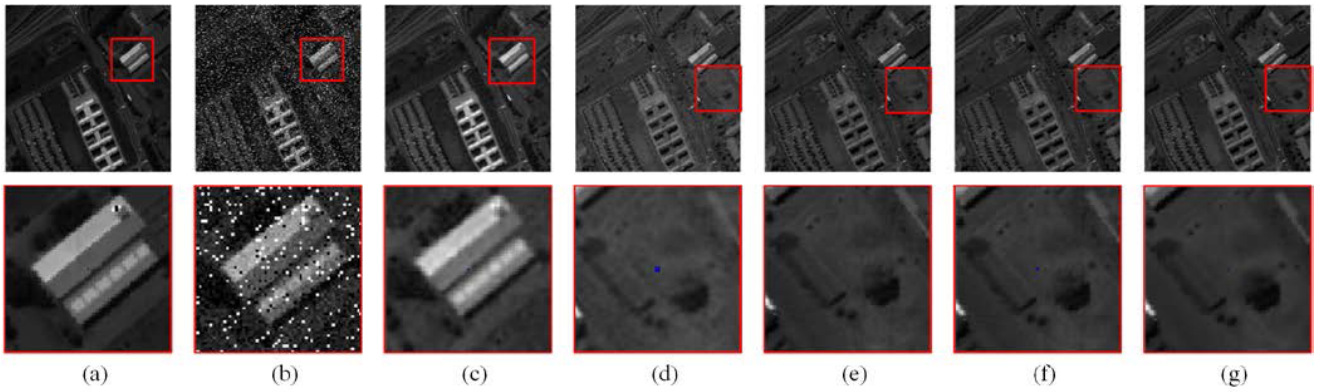

FIGURE 3. Denoising results of the 25th spectral bands in the Pavia University image: (a) Original band, (b) noisy band, (c) BM4D, (d) PARAFAC, (e) LRMR, (f) SS-LRR, (g) The proposed GSLRTD. Upper row: whole band; lower row: closeup.

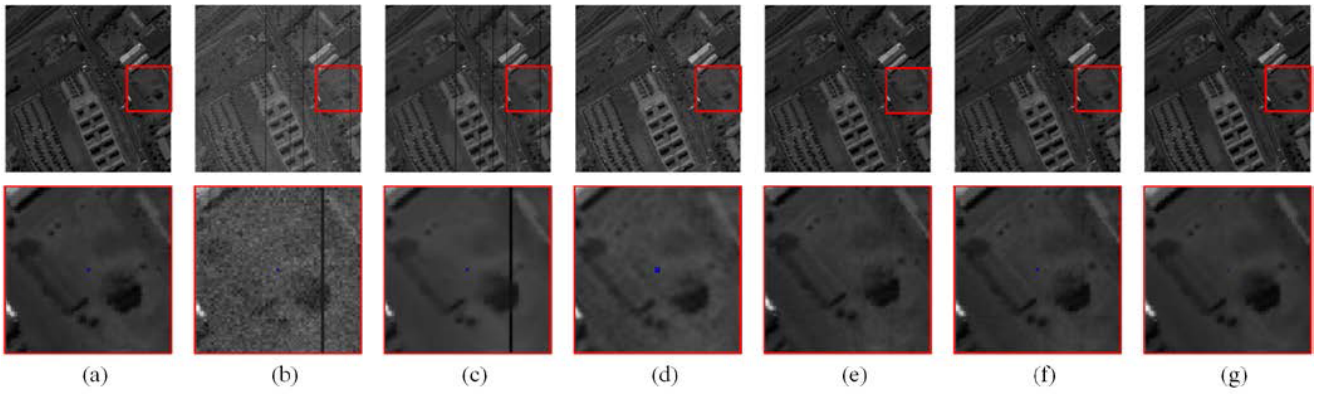

FIGURE 4. Denoising results of the 72nd spectral bands in the Pavia University image: (a) Original band, (b) noisy band, (c) BM4D, (d) PARAFAC, (e) LRMR, (f) SS-LRR, (g) The proposed GSLRTD. Upper row: whole band; lower row: closeup.

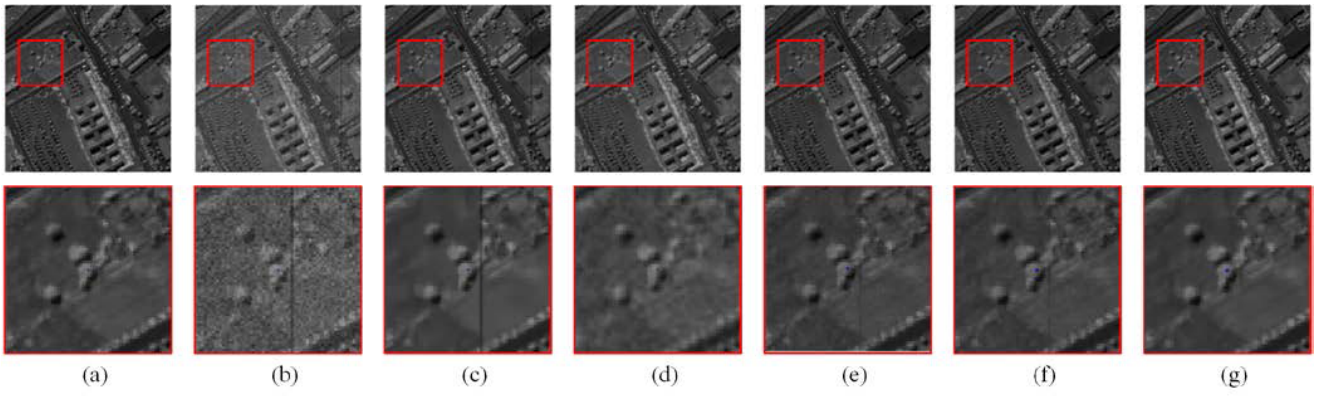

FIGURE 5. Denoising results of the 85th spectral bands in the Pavia University image: (a) Original band, (b) noisy band, (c) BM4D, (d) PARAFAC, (e) LRMR, (f) SS-LRR, (g) The proposed GSLRTD. Upper row: whole band; lower row: closeup.

SVDs of $n_1 \times n_2$ matrices. Thus, the complexity for each iteration is $O(n_1 n_2 n_3 \log(n_3) + n_{(1)} n_{(2)}^2 n_3)$. We denote that $n_{(1)} = \max(n_1, n_2)$ and $n_{(2)} = \min(n_1, n_2)$. In addition, the K-means algorithm is adopted to cluster. It is known that the computational complexity of the K-means algorithm is $O(ks^2)$, where k is the group number, and s is the number of samples $s = (M - m + 1) \times (N - n + 1)$. Therefore, the total computational complexity of GSLRTD is $O(n_1 n_2 n_3 \log(n_3) + n_{(1)} n_{(2)}^2 n_3 + ks^2)$.

IV. EXPERIMENT RESULTS AND DISCUSSION

Three remote sensing hyperspectral data sets, including the Pavia University and the Airborne Visible/Infrared Imaging Spectrometer (AVIRIS) Indian Pines and the Hyperspectral

TABLE 1. MPSNR, MSSIM and MFSIM values of the recovery result.

Method	BM4D	PARAFAC	LRMR	SS-LRR	GLRTR
MPSNR	35.26	32.62	36.87	36.87	**38.93**
MSSIM	0.87	0.87	0.96	0.94	**0.97**
MFSIM	0.94	0.91	0.97	0.97	**0.99**

Digital Imagery Collection Experiment (HYDICE) urban image, are used in our experiments. Before the recovery process, three data sets are scaled into the interval [0, 1]. In order to evaluate the performance of the proposed GSLRTD method, four well known denoising methods are selected for comparisons, i.e., BM4D [32], PARAFAC [16], LRMR [19], and SS-LRR [20]. All parameters involved in the competing methods are optimally assigned chosen as described in the reference papers.

A. SIMULATED DATA EXPERIMENTS

The Pavia University data set is used in the simulated data experiments. The whole image contains 610×340 pixels and 103 channels. A subimage of size $256 \times 256 \times 103$ is tested in our experiments. In this paper, the peak signal-to-noise ratio (PSNR), the structural similarity index metric (SSIM), and the feature similarity index measurement (FSIM) are used to give a quantitative assessment of the recovery results.

In simulated data experiments, four kinds of noise are added to the Pavia University image.

1) Gaussian noise with standard variance $\sigma = 0.05$ is added to all spectral bands;

2) 10 bands are added with impulse noise with a percentage of 10% from 21 to 30;

3) Dead lines are simulated for the five selected bands from 71 to 75. The number of dead lines is 5 and the width of dead lines is randomly chosen from one line to five lines;

4) Stripes are added to the five bands from 81 to 85. The number of stripes is 3 and the width of stripes is randomly chosen from one line to three lines.

Fig. 3, Fig. 4, and Fig. 5 respectively show denoising results of 25th, 72nd, 85th spectral bands, which are corrupted by different kinds of noise. It can be observed that the GSLRTD delivers the best performances, which effectively removes the mixed noise while preserving well spectral and spatial information. The BM4D can remove the Gaussian noise powerfully but performs poorly on the sparse noise. The PARAFAC can generally remove the sparse noise, but the removal of the Gaussian noise is not complete. The LRMR fails to remove the sparse noise totally, contributing to failure in the reconstruction of some fine structures. The SS-LRR can remove different types of noise, but it cannot well preserve the detailed structures.

In addition, we compute the PSNR, SSIM and FSIM values with each clean band and restored band, and then average them. The average values are then referred to as the mean PSNR (MPSNR), mean SSIM (MSSIM) and mean FSIM (MFSIM) indices. Table 1 presents the MPSNR, MSSIM and MFSIM values of the five denoising approaches.

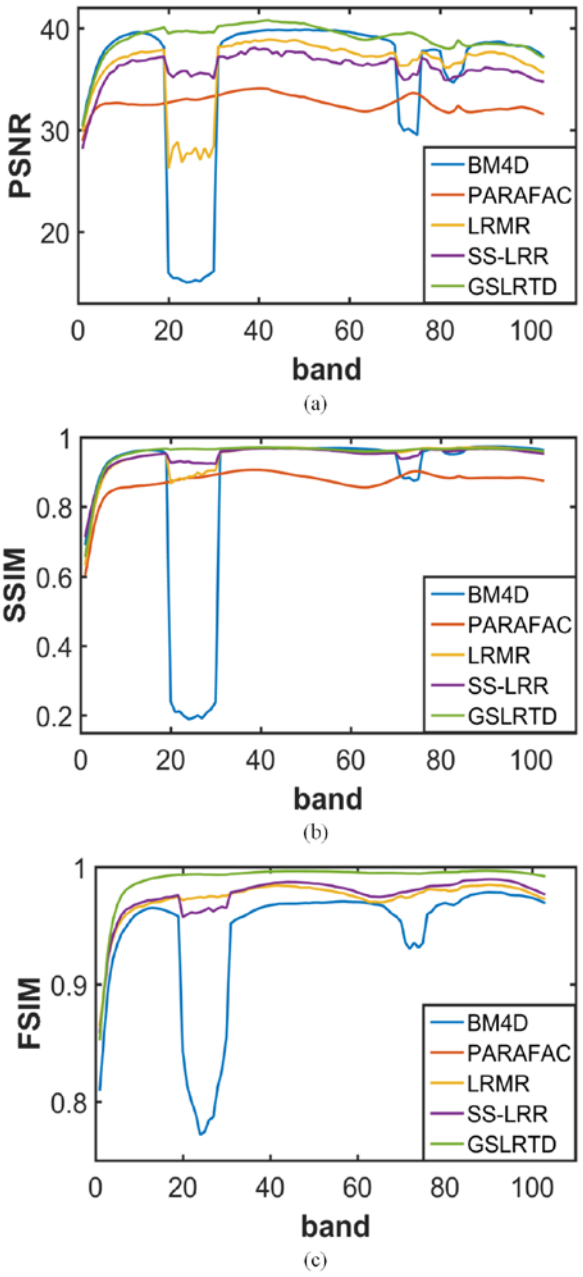

FIGURE 6. PSNR, SSIM, and FSIM values of each band of the reconstructed results on different denoising methods: (a) PSNR, (b) SSIM, and (c) FSIM.

Fig. 6 displays the band by-band PSNR, SSIM, and FSIM values of the all methods restoration results. Here, GSLRTD achieves the best PSNR, SSIM, and FSIM values in almost all the bands. It is obvious that our approach is superior to others, which demonstrates the efficiency of the nonlocal tensor strategy utilized in our method.

B. REAL HSI DATA EXPERIMENTS

1) AVIRIS INDIAN PINES IMAGE

The imagery of AVIRIS Indian Pines data set is used in our first real data experiment. The imagery of AVIRIS Indian

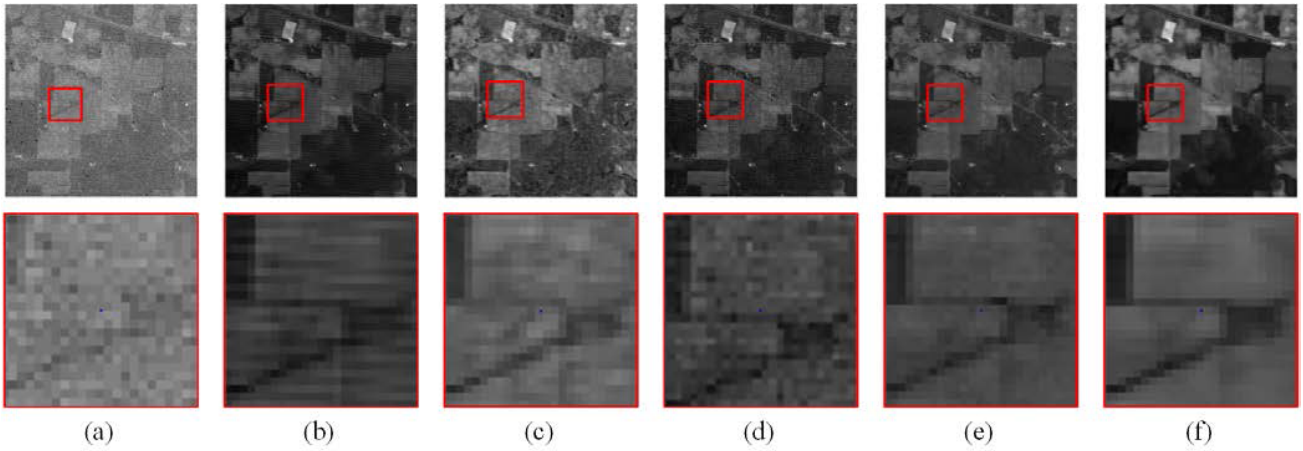

FIGURE 7. Denoising results of the 2nd spectral band in the AVIRIS Indian Pines image: (a) Original band, (b) BM4D, (c) PARAFAC, (d) LRMR, (e) SS-LRR, (f) The proposed GSLRTD. Upper row: whole band; lower row: closeup.

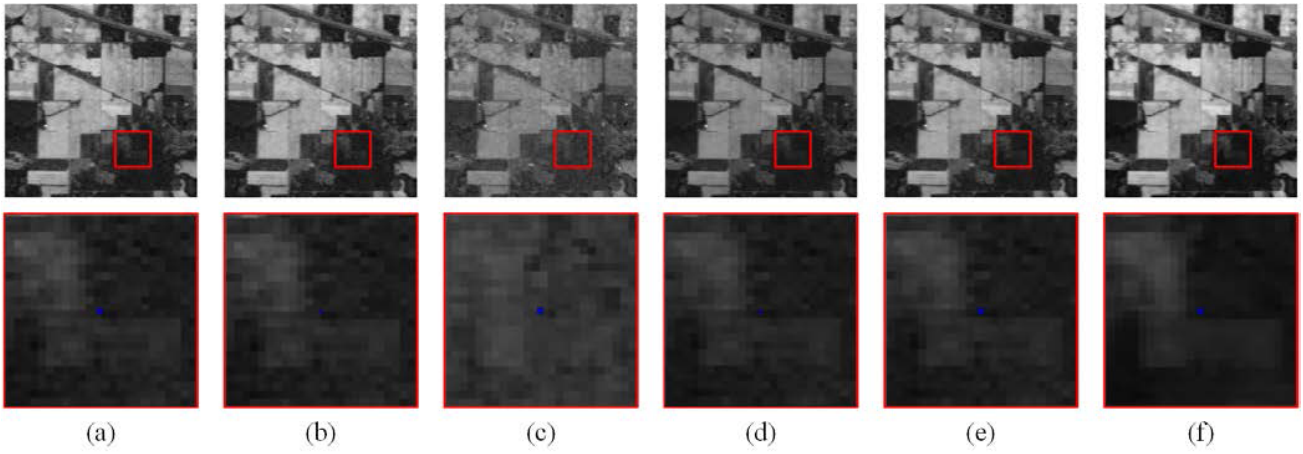

FIGURE 8. Denoising results of the 108th spectral band in the AVIRIS Indian Pines image: (a) Original band, (b) BM4D, (c) PARAFAC, (d) LRMR, (e) SS-LRR, (f) The proposed GSLRTD. Upper row: whole band; lower row: closeup.

Pines data comprises of 220 spectral bands with size of 145×145. The number of bands is reduced to 200 by removing 20 water absorption bands. Without reference noise-free images, the performance of image denoising on classification accuracy is compared. Support vector machine (SVM) [33] is adopted to conduct the classification result for the data set. The metrics of the overall accuracy (OA), average accuracy (AA) and kappa statistic [34] are used to objectively compare influence of different denoising methods. The ground truth of the data in the reference includes sixteen classes, which consists of 10249 samples. Among them, 10% of the labeled samples are randomly chosen for training and the rest 90% of the labeled samples are used for test and the details can refer to [20]. The classification process is repeated 10 times.

Fig. 7 and Fig. 8 present the recovery result images of 2nd and 108th spectral band respectively. As is shown above, when it comes to the cases of more serious noise, more obvious superiority in suppressing noise and simultaneously keeping the local details can be seen from the results by the GSLRTD. Here, the BM4D fails to recover most of the stripes. The restoration results of PARAFAC is over-smoothed, and most of the details are lost. The LRMR and SS-LRR can remove the mixed noise, but fail to efficiently preserve image details.

Classification results before and after denoising for the tested HSI are given in Table 2. Table 2 demonstrates the effectiveness of the proposed GSLRTD denoising method and the three indexes can demonstrate that the proposed GSLRTD method is superior to others. Moreover, the kappa of the proposed GSLRTD is at least 1.5% higher than the other five compared methods.

2) HYDICE URBAN IMAGE

HYDICE urban data set is used in our second real data experiment. The size of original data is $304 \times 304 \times 210$ and a subimage of size $200 \times 200 \times 210$ is selected to test. Fig. 9 illustrates the recovery result images of 206th spectral band. It can be clearly observed that the BM4D method can

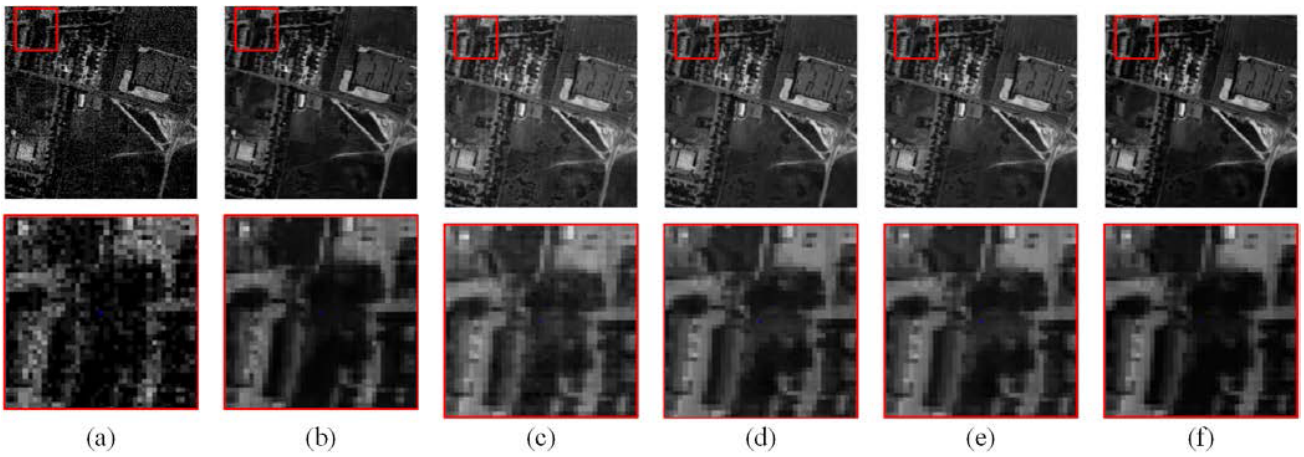

FIGURE 9. Denoising results of the 206th spectral band in the HYDICE urban image: (a) Original band, (b) BM4D, (c) PARAFAC, (d) LRMR, (e) SS-LRR, (f) The proposed GSLRTD. Upper row: whole band; lower row: closeup.

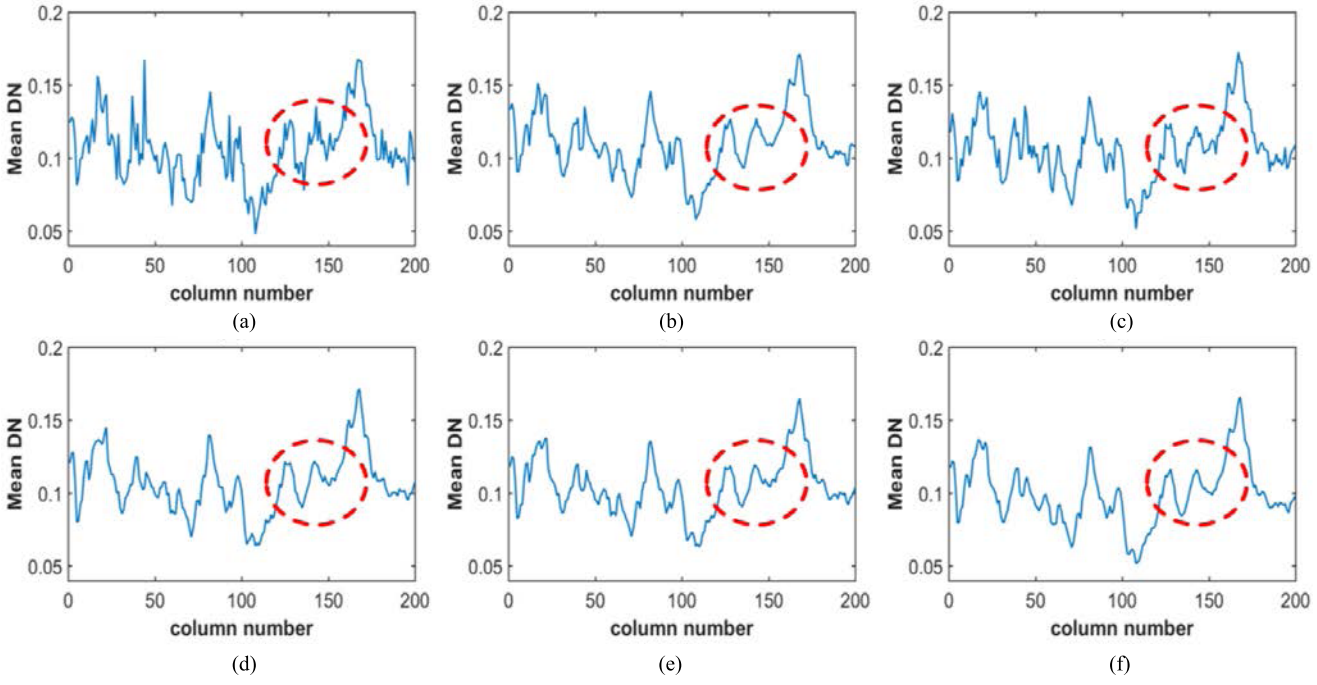

FIGURE 10. Vertical mean profiles of denoising results of the 206th spectral band in the HYDICE urban image: (a) Original band, (b) BM4D, (c) PARAFAC, (d) LRMR, (e) SS-LRR, (f) The proposed GSLRTD.

well remove the Gaussian noise, but fail to effectively remove the stripes. The PARAFAC can more or less remove the stripes, but it causes the denoised results to be oversmoothed. The LRMR and SS-LRR perform better than BM4D and PARAFAC, but some image details cannot be well preserved. The GSLRTD performs best, eliminating most of the mixed noise and reconstructing the spatial details.

To further compare the performances of all the restoration algorithms, the vertical mean profiles [22] of 206th spectral band before and after reconstruction is displayed in Fig. 10. The horizontal axis in Fig. 10 represents the column number, and the vertical axis represents the mean digital number (mean DN) value of each column. Due to the influence of stripes, there is violent fluctuation in the curve. After the denoising processing, the fluctuation become more or less smooth and steady. However, the BM4D and PARAFAC fail to restore the image in some regions. Compared to the results of LRMR and SS-LRR, our method provides smoother curve, which represents that the stripes have been more effectively removed.

TABLE 2. Classification accuracies (%) of indian pines image obtained by different methods.

Class	SVM	BM4D	PARAFAC	LRMR	SS-LRR	GSLRTR
1	88.96	90.46	88.55	92.27	**93.21**	90.69
2	74.51	78.75	77.83	82.51	81.65	**83.51**
3	71.47	76.08	74.34	74.44	78.89	**85.82**
4	86.87	88.67	**89.26**	88.59	88.85	88.65
5	90.78	93.88	91.94	91.39	96.63	**97.76**
6	96.89	**98.02**	97.21	97.53	97.89	97.36
7	92.62	93.61	94.41	94.83	94.56	**96.83**
8	96.23	98.41	99.04	98.32	98.99	**99.72**
9	93.69	97.98	**98.08**	97.18	97.66	96.47
10	78.09	83.26	81.35	82.26	83.17	**87.31**
11	72.23	82.49	80.16	83.21	83.78	**84.17**
12	70.37	82.26	80.19	84.33	82.15	**84.49**
13	97.33	98.75	99.02	98.78	98.35	**99.13**
14	93.61	97.44	95.28	96.22	**98.96**	98.84
15	63.02	70.96	68.39	72.35	72.17	**74.81**
16	97.25	96.32	97.74	97.58	**98.21**	98.15
AA	85.24	89.36	88.31	89.47	90.86	**91.48**
OA	81.44	85.34	84.91	88.15	89.32	**90.53**
Kappa	0.785	0.839	0.831	0.857	0.871	**0.884**

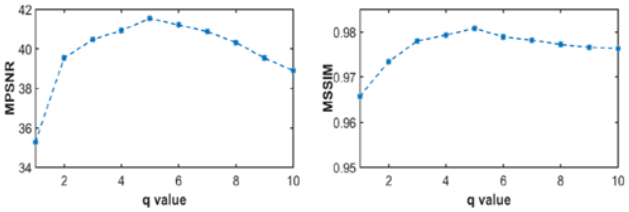

FIGURE 11. Analysis of parameter $\lambda(\lambda = q/\sqrt{\max(M,N)P})$ q is changed from 1 to 10). (a) The relationship between MPSNR and q value. (b) The relationship between MSSIM and q value.

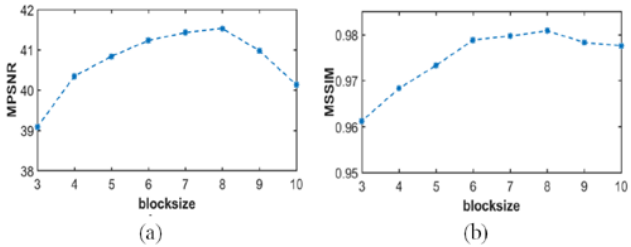

FIGURE 12. Analysis of blocksize l (l is changed from 3 to 10). (a) The relationship between MPSNR and the blocksize l. (b) The relationship between MSSIM and the blocksize l.

C. PARAMETERS DISCUSSIONS

There are two parameters mainly involved in GSLRTD: the sparsity regularization parameter λ and blocksize l. In all the experiments with GSLRTD algorithm, we set the sparsity regularization parameter λ and blocksize l as $\lambda = 5/\sqrt{\max(M,N)P}$ and $l = 8$. In this subsection, we use the metrics of MPSNR and MSSIM to evaluate the influence of two parameters on denoising results. All the experiments are based on the simulated data experiment, the Pavia University data set.

Sensitivity Analysis of Parameter λ: In (12), λ serves as the parameter to confine the sparsity of the sparse noise. As in the GSLRTD model, the sparsity regularization parameter is set to $\lambda = 1/\sqrt{\max(M,N)P}$, which is an important regulation parameter to remove noise. In Fig. 11, we set $\lambda = q/\sqrt{\max(M,N)P}$ and q is changed from a set of [1,2,3,4,5,6,7,8,9,10]. It can be observed that MPSNR and MSSIM are relatively stable when q is changed from 4 to 7.

Blocksize l: l is related to the size of nonlocal similarity cubes. The experimental results of MPSNR and MSSIM with the blocksize l are showed in Fig. 12. The λ is fixed at $\lambda = 5/\sqrt{\max(M,N)P}$ and we can observe that when $l = 8$, the GSLRTD method achieves the best denoising performance.

V. CONCLUSIONS

In this paper, we propose a novel group sparse and low-rank tensor decomposition (GSLRTD) denoising method to remove the mixed noise in hyperspectral image. In addition, a sparse and low-rank tensor decomposition model is adopted to remove the mixed noise in the HSI, while preserving well spectral and spatial characteristics. Experimental results demonstrate the proposed method outperforms well known denoising methods. In our future work, we will consider using the total variation regularization to better recover spatial structure and texture of HSI.

ACKNOWLEDGMENT

The authors would like to thank Prof. D. A. Landgrebe of Purdue University along with the NASA Jet Propulsion Laboratory for providing the free downloads of the hyperspectral data sets. In addition, we would like to thank Dr. J. Ma for providing the software for the SS-LRR method.

REFERENCES

[1] L. Lei, H. Min, and Q. Tie, "Remote sensing image classification based on ensemble extreme learning machine with stacked autoencoder," *IEEE Access*, vol. 5, pp. 9021–9031, May 2017.
[2] F. L. Peña, J. L. Crespo, and R. J. Duro, "Unmixing low-ratio endmembers in hyperspectral images through Gaussian synapse ANNs," *IEEE Trans. Instrum. Meas.*, vol. 59, no. 7, pp. 1834–1840, Jul. 2010.
[3] M. D. Iordache, J. M. Bioucas, and A. Plaza, "Sparse unmixing of hyperspectral data," *IEEE Trans. Geosci. Remote Sens.*, vol. 49, no. 6, pp. 2014–2039, Jun. 2011.
[4] H. Liu and S. Li, "Target detection using sparse representation with element and construction combination feature," *IEEE Trans. Instrum. Meas.*, vol. 64, no. 2, pp. 290–298, Feb. 2015.
[5] H. Liu, S. Li, and L. Fang, "Robust object tracking based on principal component analysis and local sparse representation," *IEEE Trans. Instrum. Meas.*, vol. 64, no. 11, pp. 2863–2875, Nov. 2015.
[6] C. Bo, H. Lu, and D. Wang, "Weighted generalized nearest neighbor for hyperspectral image classification," *IEEE Access*, vol. 5, pp. 1496–1509, Feb. 2017.
[7] W. Yang, K. Hou, B. Liu, F. Yu, and L. Lin, "Two-stage clustering technique based on the neighboring union histogram for hyperspectral remote sensing images," *IEEE Access*, vol. 5, no. 4, pp. 5640–5647, Apr. 2017.
[8] L. Fang, C. Wang, S. Li, and J. A. Benediktsson, "Hyperspectral image classification via multiple-feature-based adaptive sparse representation," *IEEE Trans. Instrum. Meas.*, vol. 66, no. 7, pp. 1646–1657, Jul. 2017.
[9] Y. Wang, Y. Shao, Z. Gui, Q. Zhang, L. Yao, and Y. Liu, "A novel fractional-order differentiation model for low-dose CT image processing," *IEEE Access*, vol. 4, pp. 8487–8499, 2016.
[10] B. Rasti, J. R. Sveinsson, M. O. Ulfarsson, and J. A. Benediktsson, "Hyperspectral image denoising using first order spectral roughness penalty in wavelet domain," *IEEE J. Sel. Topics Appl. Earth Observat. Remote Sens.*, vol. 7, no. 6, pp. 2458–2467, Jun. 2014.

[11] S. R. Thatiparthi, R. R. Gudheti, and V. Sourirajan, "MST radar signal processing using wavelet-based denoising," *IEEE Geosci. Remote Sens. Lett.*, vol. 6, no. 4, pp. 752–756, Oct. 2009.
[12] M. Cheng, C. Wang, and J. Li, "Sparse representation based pansharpening using trained dictionary," *IEEE Geosci. Remote Sens. Lett.*, vol. 11, no. 1, pp. 293–297, Jan. 2014.
[13] Q. Yuan, L. Zhang, and H. Shen, "Hyperspectral image denoising employing a spectral–spatial adaptive total variation model," *IEEE Trans. Geosci. Remote Sens.*, vol. 50, no. 10, pp. 3660–3677, Oct. 2012.
[14] K. Dabov, A. Foi, V. Katkovnik, and K. Egiazarian, "Image denoising by sparse 3-D transform-domain collaborative filtering," *IEEE Trans. Image Process.*, vol. 16, no. 8, pp. 2080–2095, Aug. 2007.
[15] D. Letexier and S. Bourennane, "Noise removal from hyperspectral images by multidimensional filtering," *IEEE Trans. Geosci. Remote Sens.*, vol. 46, no. 7, pp. 2061–2069, Jul. 2008.
[16] X. Liu, S. Bourennane, and C. Fossati, "Nonwhite noise reduction in hyperspectral images," *IEEE Geosci. Remote Sens. Lett.*, vol. 9, no. 3, pp. 368–372, May 2012.
[17] L. Liu, L. Chen, C. L. P. Chen, Y. Y. Tang, and C. M. Pun, "Weighted joint sparse representation for removing mixed noise in image," *IEEE Trans. On Cyber.*, vol. 47, no. 3, pp. 600–611, Mar. 2016.
[18] B. Xiong and Z. Yin, "A universal denoising framework with a new impulse detector and nonlocal means," *IEEE Trans. Image Process.*, vol. 21, no. 4, pp. 1663–1675, Apr. 2012.
[19] H. Zhang, W. He, L. Zhang, H. Shen, and Q. Yuan, "Hyperspectral image restoration using low-rank matrix recovery," *IEEE Trans. Geosci. Remote Sens.*, vol. 52, no. 8, pp. 4729–4743, Aug. 2014.
[20] F. Fan, Y. Ma, C. Li, X. Mei, J. Huang, and J. Ma, "Hyperspectral image denoising with superpixel segmentation and low-rank representation," *Inf. Sci.*, vols. 397–398, pp. 48–68, Aug. 2017.
[21] M. Wang, Y. Jing, J. Xue, and W. Sun, "Denoising of hyperspectral images using group low-rank representation," *IEEE J. Sel. Topics Appl. Earth Observ. Remote Sens.*, vol. 9, no. 9, pp. 4420–4427, Sep. 2016.
[22] W. He, H. Zhang, L. Zhang, and H. Shen, "Total-variation-regularized low-rank matrix factorization for hyperspectral image restoration," *IEEE Trans. Geosci. Remote Sens.*, vol. 54, no. 1, pp. 178–188, Jan. 2016.
[23] X. Guo, X. Huang, L. Zhang, and L. Zhang, "Hyperspectral image noise reduction based on rank-1 tensor decomposition," *ISPRS J. Photogram. Remote Sens.*, vol. 83, no. 1, pp. 50–63, Sep. 2013.
[24] H. Fan, Y. Chen, Y. Guo, H. Zhang, and G. Kuang, "Hyperspectral image restoration using low-rank tensor recovery," *IEEE J. Sel. Topics Appl. Earth Observ. Remote Sens.*, vol. 10, no. 10, pp. 4589–4604, Oct. 2017.
[25] Z. Wu, Q. Wang, J. Jin, and Y. Shen, "Structure tensor total variation-regularized weighted nuclear norm minimization for hyperspectral image mixed denoising," *Signal Process.*, vol. 131, no. 1, pp. 202–219, Feb. 2017.
[26] E. J. Candès, X. Li, Y. Ma, and J. Wright, "Robust principal component analysis?" *J. ACM*, vol. 58, no. 3, pp. 1–37, May 2011.
[27] X. Yuan and J. Yang, "Sparse and low-rank matrix decomposition via alternating direction methods," *Pacific J. Optim.*, vol. 9, no. 1, pp. 167–180, 2013.
[28] T. G. Kolda and B. W. Bader, "Tensor decompositions and applications," *SIAM Rev.*, vol. 51, no. 3, pp. 455–500, 2009.
[29] C. Lu, J. Feng, Y. Chen, W. Liu, Z. Lin, and S. Yan, "Tensor robust principal component analysis: Exact recovery of corrupted low-rank tensors via convex optimization," in *Proc. IEEE Conf. Comput. Vis. Pattern Recognit.*, Jun. 2016, pp. 5249–5257.
[30] Z. Zhang, G. Ely, S. Aeron, N. Hao, and M. Kilmer, "Novel methods for multilinear data completion and de-noising based on tensor-SVD," in *Proc. IEEE Conf. Comput. Vis. Pattern Recognit.*, Jun. 2014, pp. 3842–3849.
[31] D. Arthur and S. Vassilvitskii, "K-means++: The advantages of careful seeding," in *Proc. Annu. ACM-SIAM Symp. Discrete Algorithms*, vol. 11, no. 6, pp. 1027–1035, Jun. 2007.
[32] M. Maggioni, V. Katkovnik, K. Egiazarian, and A. Foi, "Nonlocal transform-domain filter for volumetric data denoising and reconstruction," *IEEE Trans. Image Process.*, vol. 22, no. 1, pp. 119–133, Jan. 2013.
[33] R. Archibald and G. Fann, "Feature selection and classification of hyperspectral images with support vector machines," *IEEE Geosci. Remote Sens. Lett.*, vol. 4, no. 4, pp. 674–677, Oct. 2007.
[34] L. Fang, S. Li, X. Kang, and J. A. Benediktsson, "Spectral–spatial hyperspectral image classification via multiscale adaptive sparse representation," *IEEE Trans. Geosci. Remote Sens.*, vol. 52, no. 12, pp. 7738–7749, Dec. 2014.

ZHIHONG HUANG received the B.Sc. degree from the Hunan University of Science and Technology, Xiangtan, China, in 2015. He is currently pursuing the Ph.D. degree in control science and engineering with Hunan University, Changsha, China. His research interests include hyperspectral image denoising and classification.

SHUTAO LI (M'07–SM'15) received the B.S., M.S., and Ph.D. degrees in electrical engineering from Hunan University, Changsha, China, in 1995, 1997, and 2001, respectively. He was a Research Associate with the Department of Computer Science, The Hong Kong University of Science and Technology, Hong Kong, in 2001.

From 2002 to 2003, he was a Post-Doctoral Fellow with the Royal Holloway College, University of London, London, U.K., under the supervision of Prof. J. Shawe-Taylor. In 2005, he was a Visiting Professor with the Department of Computer Science, The Hong Kong University of Science and Technology. He joined the College of Electrical and Information Engineering, Hunan University, in 2001, where he is currently a Full Professor. He has authored or co-authored over 160 refereed papers. His current research interests include compressive sensing, sparse representation, image processing, and pattern recognition.

Dr. Li is a member of the Editorial Board of the Information Fusion and the Sensing and Imaging. He was a recipient of two Second-Grade National Awards at the Science and Technology Progress of China in 2004 and 2006, respectively. He is currently an Associate Editor of the IEEE TRANSACTIONS ON GEOSCIENCE AND REMOTE SENSING and the IEEE TRANSACTIONS ON INSTRUMENTATION AND MEASUREMENT.

LEYUAN FANG (M'14–SM'17) received the B.S. and Ph.D. degrees from the College of Electrical and Information Engineering, Hunan University, Changsha, China, in 2008 and 2015, respectively.

From 2011 to 2012, he was a Visiting Ph.D. Student with the Department of Ophthalmology, Duke University, Durham, NC, USA, supported by the China Scholarship Council. Since 2017, he has been an Associate Professor with the College of Electrical and Information Engineering, Hunan University. His research interests include sparse representation and multiresolution analysis in remote sensing and medical image processing. He received the Scholarship Award for the Excellent Doctoral Student from the Chinese Ministry of Education in 2011.

HUALI LI (M'14) received the B.S. degree from Wuhan University, Wuhan, China, in 2007, and the Ph.D. degree in photogrammetry and remote sensing from the State Key Laboratory of Information Engineering in Surveying, Mapping and Remote Sensing, Wuhan University, in 2012.

She has been an Assistant Professor with the College of Electrical and Information Engineering, Hunan University, China, since 2012. Her major research interests include pattern recognition, hyperspectral image processing, and signal processing.

JÓN ATLI BENEDIKTSSON (S'84–M'90–SM'99–F'04) received the Cand.Sci. degree from the University of Iceland, Reykjavik, Iceland, in 1984, and the M.S.E.E. and Ph.D. degrees from Purdue University, West Lafayette, IN, USA, in 1987 and 1990, respectively, all in electrical engineering. From 2009 to 2015, he was the Pro Rector of Science and Academic Affairs and a Professor of electrical and computer engineering with the University of Iceland. In 2015, he became the Rector of the University of Iceland. He is the Co-Founder of a biomedical startup company Oxymap. He has authored extensively in his fields of interest. His research interests include remote sensing, image analysis, pattern recognition, biomedical analysis of signals, and signal processing. He is a member of the 2014 IEEE Fellow Committee. He is a fellow of the International Society for Optics and Photonics. He was President of the IEEE Geoscience and Remote Sensing Society (GRSS) from 2011 to 2012. He has been on the GRSS Administrative Committee since 2000. He was the Chairman of the Steering Committee of the IEEE Journal of Selected Topics in Applied Earth Observations and Remote Sensing from 2007 to 2010. He serves on the Editorial Board of the IEEE Proceedings and the International Editorial Board of the *International Journal of Image and Data Fusion*. He was a recipient of the Stevan J. Kristof Award from Purdue University in 1991 as an Outstanding Graduate Student in remote sensing. He was also a recipient of the Icelandic Research Councils Outstanding Young Researcher Award in 1997, the IEEE Third Millennium Medal in 2000, the Yearly Research Award from the Engineering Research Institute at the University of Iceland in 2006, the Outstanding Service Award from the IEEE Geoscience and Remote Sensing Society in 2007, and the IEEE/VFI Electrical Engineer of the Year Award in 2013. He was a co-recipient of the University of Iceland's Technology Innovation Award in 2004, the 2012 IEEE Transactions on Geoscience and Remote Sensing Paper Award, the IEEE GRSS Highest Impact Paper Award in 2013, and the *International Journal of Image and Data Fusion* Best Paper Award in 2014. He was the Editor-in-Chief of the IEEE Transactions on Geoscience and Remote Sensing (TGRS) from 2003 to 2008. He has been an Associate Editor of TGRS since 1999, the IEEE Geoscience and Remote Sensing Letters since 2003, and IEEE Access since 2013.